Journal of
Clinical Medicine

MDPI

Review

Blood Speckle Tracking Echocardiography in Congenital Heart Disease: Current Applications, Emerging Flow Signs, and Future Perspectives: An Opinion Review

Massimiliano Cantinotti, Pietro Marchese, Guglielmo Capponi *, Cecilia Viacava, Giulia Corana, Eliana Franchi, Giuseppe Santoro and Nadia Assanta

Fondazione G. Monasterio CNR-Regione Toscana, 56124 Pisa, Italy
* Correspondence: capponi@ftgm.it

Abstract

Blood speckle tracking (BST) echocardiography is an emerging ultrafast ultrasound-based imaging technique that enables visualization of blood-flow patterns in cardiac chambers and great vessels. In the studies reviewed here, acquisition and flow tracking are predominantly performed in two-dimensional imaging planes and across time; therefore, the term "4D" should not be interpreted as a validated, fully volumetric three-dimensional flow acquisition. By exploiting high-frame-rate plane-wave imaging, BST allows angle-independent reconstruction of multidirectional flow vectors, vortex formation, turbulent propagation, and flow energetics, providing hemodynamic information beyond that obtainable with conventional Doppler echocardiography. This capability is particularly relevant in fetuses, neonates, and children with congenital heart disease (CHD), in whom altered chamber geometry, abnormal loading conditions, and complex postoperative anatomies frequently generate non-laminar flow patterns, recirculation zones, and pathological vortices. Over the last few years, studies have reported high feasibility of BST in selected pediatric and fetal populations, with successful acquisition rates exceeding 90% in several cohorts. However, feasibility estimates vary by study, population, imaging plane, and endpoint, and reproducibility and clinical validity remain incompletely established. Current applications include assessment of ventricular vortex morphology, energy loss, intraventricular pressure differences, aortic and pulmonary flow patterns, and characterization of altered hemodynamics in complex CHD, including bicuspid aortic valve disease, tetralogy of Fallot, coarctation of the aorta, cardiomyopathies, and single ventricle physiology. Early studies suggest that BST-derived parameters, such as vorticity, kinetic energy, vector complexity, and pressure gradients, may provide incremental pathophysiological and potentially prognostic information beyond conventional echocardiographic metrics. Despite its promising clinical potential, widespread implementation of BST remains limited by restricted software availability, limited penetration depth, lack of standardized quantitative reference values, and the still limited evidence regarding its diagnostic and prognostic superiority over standard imaging techniques. This review provides an up-to-date overview of the technical principles, current clinical applications, hemodynamic insights, and future perspectives of BST echocardiography in congenital heart disease.

Keywords: blood speckle tracking; echocardiography; children; 4D echocardiography; vortex analysis

Check for updates

Academic Editor: Donald J. Hagler

Received: 15 October 2026
Revised: 1 November 2026
Accepted: 6 November 2026
Published: 16 November 2026

Copyright: © 2026 by the authors. Licensee MDPI, Basel, Switzerland. This article is an open access article distributed under the terms and conditions of the Creative Commons Attribution (CC BY) license.

1. Introduction

Blood speckle tracking (BST) echocardiography is a relatively novel echocardiographic technique [1–9] that enables visualization of blood-flow trajectories and vortex formation within cardiac chambers and the main vessels. Although BST sequences depict flow over time, most currently described clinical applications use two-dimensional imaging planes rather than volumetric three-dimensional acquisition. Accordingly, "4D flow" is used cautiously in this review as a broad descriptive label, not as a claim that out-of-plane flow is captured. First introduced into pediatric cardiovascular imaging in 2019–2021 [1,2,4,6,7], BST has rapidly emerged as a promising tool for the assessment of intracardiac flow dynamics in fetuses and children with congenital heart disease (CHD).

In contrast to conventional echocardiography, which mainly provides structural information and beam-dependent velocity data, BST allows a direct and intuitive visualization of complex multidirectional flow phenomena, including vortex formation, helical flow, post-stenotic turbulence, and intracavitary recirculation zones [1–8]. These flow patterns are particularly relevant in CHD, where abnormal geometry and altered pressure–volume loading conditions significantly influence hemodynamics [1–8].

BST acquisition is rapid, highly reproducible, and relatively easy to integrate into routine pediatric echocardiographic practice [1–8]. Nevertheless, several important limitations persist. At present, the technology is mainly available on pediatric transthoracic and transesophageal probes, which limits penetration depth and currently restricts its use primarily to fetal and pediatric populations [1–9]. Furthermore, while several advanced quantitative parameters such as vorticity, vector complexity, kinetic energy, energy loss, and intraventricular pressure differences have been developed in research settings, most of these software tools are not yet commercially available [1–9].

The aim of this review is to provide an updated overview of BST echocardiography, focusing on its technical principles, feasibility, and current clinical applications in pediatric and fetal congenital heart disease, with particular attention to emerging visual flow signs and to the distinction between BST evidence and findings obtained using other flow-imaging methods.

Building on our previous review (10), this article updates the evidence from recent fetal and pediatric studies, examines selected quantitative findings, and critically discusses emerging signs such as the proposed stop-flow sign. Some figures in this manuscript reproduce or adapt material from the previous review [10]. Reproduced or adapted material is identified in the relevant figure captions; permissions and any overlapping Supplementary Materials must be verified before submission.

2. Materials and Methods

A literature search was conducted in 18 January 2026 using PubMed/MEDLINE, ScienceDirect, and the Cochrane Library. The search combined the following free-text terms and, where available, controlled vocabulary: ("echocardiography" OR "ultrasound") AND ("blood speckle tracking" OR "blood speckle imaging" OR "high-frame-rate ultrasound") AND ("children" OR "fetal" OR "congenital heart disease").

Additional searches combined the BST terms with "ventricle", "vortex", "energy loss", "intraventricular pressure difference", "cardiomyopathy", "single ventricle", "aortic", and "pulmonary". The exact search strings and database-specific syntax were not prospectively archived; this limitation should be considered when interpreting the search as reproducible.

Potentially relevant studies were also identified through manual screening of the reference lists of all eligible articles and review papers, as well as through citation tracking using the Science Citation Index Expanded (Web of Science).

Titles and abstracts were screened for relevance, and potentially eligible full texts were assessed. Studies were excluded from the BST-focused evidence synthesis if they (a) used non-echocardiographic imaging, (b) used echocardiographic flow methods other than BST, or (c) were not published in English. Studies using other echocardiographic flow-reconstruction methods or cardiovascular magnetic resonance were retained only as contextual evidence and are identified as such in the text.

This is an opinion review with a narrative synthesis, not a systematic review. PRISMA 2020 (https://www.prisma-statement.org/) compliance is therefore not claimed, and the search should be regarded as a structured, but not fully reproducible, literature search.

The selected articles were evaluated by specialists in pediatric echocardiography (M.C. and P.M.), and inclusion was based on consensus. Because a complete database-by-database search log and deduplicated screening record were not available, the study-selection counts and Figure 1 must be reconciled against the original search records before submission.

Stage	Selection process	n
Identification	Records identified through PubMed/MEDLINE, ScienceDirect and Cochrane Library	**42**
Additional identification	Studies identified through manual screening of reference lists and citation tracking	Not quantified
Screening	Records screened by title and abstract	**42**
	Records excluded	**21**
Eligibility	Full-text articles assessed for eligibility	**21**
Full-text exclusion	Studies using imaging modalities other than echocardiography	**15**
	Studies published in languages other than English	**1**
	Studies evaluating echocardiographic 4D-flow techniques, including vector flow imaging, published before BST	**5**
Included	Studies included in the final qualitative analysis	**21**

Figure 1. Inclusion/exclusion criteria.

Use of anonymized videos and images was approved by the local ethics committee, FTGM CE (approval code: Study "Bet" No. 390). Parents or legal guardians were duly informed and provided with written informed consent.

3. Results

The search identified 42 records before final screening. A total of 42 publications were initially identified through the search strategy. After title, abstract, and full-text screening, 21 studies met the predefined inclusion criteria and were included in the final analysis.

A total of 21 articles were excluded, including 15 studies using imaging modalities other than echocardiography, 1 study published in languages other than English, and 5 that evaluated echocardiographic 4D flow techniques (e.g., vector flow imaging) anterior to BST.

3.1. Ultrafast Echo Imaging: Technical Principles, Feasibility, and Current Clinical Evidence

Blood speckle tracking (BST) echocardiography is based on ultrafast non-focused plane wave ultrasound technology, which represents a substantial technical evolution compared with conventional echocardiographic imaging [1–12]. While standard echocardiography

relies on sequential focused beam transmission along multiple scan lines, thereby inherently limiting temporal resolution, ultrafast imaging employs the transmission of a non-focused plane wave across the entire imaging sector [1–10,12]. This approach enables the simultaneous insonation of the whole field of view with a single emission, allowing extremely high acquisition rates, typically ranging from 2500 to 5000 frames per second (fps) [1–9,12,13]. For practical display and offline analysis, frame rates are usually reduced to approximately 400–600 fps, while preserving the temporal information required for flow tracking [1–8].

This very high temporal resolution is the fundamental prerequisite for blood speckle tracking, as it allows frame-by-frame tracking of the natural acoustic speckle generated by circulating erythrocytes [1–9,12,13]. Through dedicated tracking algorithms, BST reconstructs multidirectional blood flow vectors and provides real-time visualization of intracardiac flow trajectories, vortex formation, recirculation zones, and turbulent flow propagation [1,9,12,13]. One of the major advantages of this technique is its relative angle independence, which overcomes one of the intrinsic limitations of conventional Doppler imaging, namely the dependency of velocity estimation on alignment with the ultrasound beam [1,9,12,13].

From a clinical perspective, ultrafast imaging is particularly attractive because it combines rapid acquisition with intuitive visualization of complex hemodynamic patterns, making it especially useful in congenital heart disease (CHD), where multidirectional flow jets, abnormal vortices, and post-stenotic turbulence are common. BST acquisition is performed similarly to standard color Doppler imaging and is fast, fully non-invasive, and easy to perform [1,2]. To obtain a BST movie, the operator selects the BST mode from the color Doppler interface and stores the image. Post-processing is equally rapid: by activating the "show particles" function, the software automatically reconstructs the vortex-based flow movie. The entire workflow, from acquisition to reconstruction, takes only a few seconds. High-quality BST recordings can be obtained under normal clinical conditions, without the need for sedation [1,2].

However, despite these advantages, some important technical limitations remain. Because BST currently relies mainly on high-frequency pediatric transthoracic and transesophageal probes, tissue penetration remains limited, and the technique is presently most feasible at relatively shallow depths, generally below 10–12 cm. Therefore, its current clinical application is mainly restricted to fetuses, neonates, infants, and children, or to transesophageal echocardiographic studies. Commercially available probes most employed include 8 and 12 MHz transthoracic phased-array probes and the 6VT-D transesophageal probe, with performance being optimal in small body sizes and superficial cardiac structures.

3.2. Feasibility

The feasibility of this technology in pediatric populations has been convincingly demonstrated. In the initial feasibility study by Nyrnes and colleagues [1], 102 subjects aged 21 weeks to 11.5 years were prospectively enrolled, including 4 healthy fetuses, 51 healthy controls, and 47 patients with different cardiac diseases. Flow patterns in the area of interest were visualized in all but one case (>99%). This study assessed technical feasibility and should not be conflated with the later Marchese et al. cohort of 118 healthy children and 43 children with CHD [8], in which feasibility of ventricular vortex imaging was 93.7% and 95.6%, respectively.

3.3. BST Applications in Different Diseases

In the following sections, we will analyze the possible use of BST in different diseases and clinical scenarios.

3.3.1. Vortex in the Ventricles

BST has provided important insights into ventricular flow organization and vortex morphology. In the study by Marchese, Cantinotti, and colleagues, left ventricular vortex analysis was performed in healthy children and in patients with CHD [8]. After propensity score matching, there were no overall statistically significant differences in vortex position or dimensions, including distance from the apex, distance from the interventricular septum, height, width, sphericity index, or area [8]. In multivariable analyses, however, LV morphology was associated with vortex characteristics, and CHD involving LV volume or pressure overload was associated with vortices located closer to the interventricular septum [8]. The authors also reported an association between indexed vortex area and abnormal LV morphology; this exploratory finding requires external validation and should not be interpreted as an established predictive biomarker [8]. Furthermore, CHD conditions characterized by left ventricular volume or pressure overload were associated with vortices located closer to the interventricular septum, supporting the concept that altered chamber geometry directly affects intracavitary flow organization [8]. Figure 2 and Movie S1.

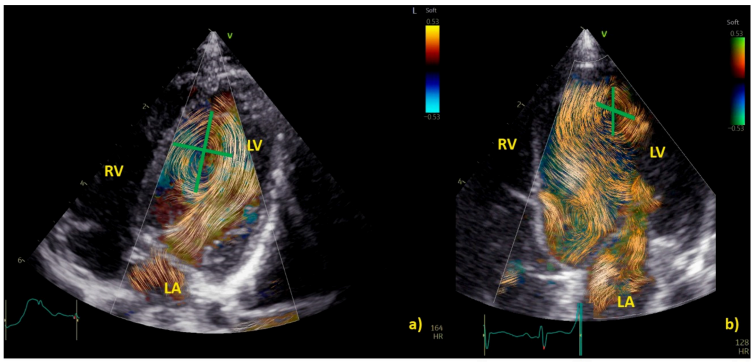


Figure 2. (**a**) and Movie S1 show the normal diastolic vortex within the left ventricle (LV) in a healthy heart. Figure 2b illustrates the diastolic vortex in a patient with left ventricular volume overload secondary to a significant patent ductus arteriosus. BST images were acquired using a zoomed apical four-chamber view, including both the interventricular septum (IVS) and the mitral valve. Vortex position was assessed in relation to two reference axes: (1) a longitudinal line from the ventricular apex to the mitral valve, and (2) a transverse line from the IVS to the LV free wall. Vortex height was defined as the longitudinal extent of the main vortex relative to LV length, while vortex width was defined as its transverse extent relative to LV width. In the pathological condition (**b**), the vortex shows a different size and spatial distribution, being located further from the interventricular septum and occupying a larger area compared with the healthy counterpart.

The application of BST in fetal cardiology has further expanded the potential of this technology. In a prospective cross-sectional study by Liu et al. [13], 35 fetuses with tetralogy of Fallot and 35 gestational-age-matched controls were analyzed. Fetuses with ToF exhibited significantly larger and longer-lasting vortices in the right ventricle compared with controls (all $p < 0.05$). Linear regression analysis demonstrated that the right ventricular vortex area was positively correlated with right ventricular sphericity index, isovolumic relaxation time, and myocardial performance index (all $p < 0.001$) [13]. In fetuses with severe ToF, the vortex was located significantly closer to the apex, while the left ventricular vortex area was also significantly increased compared with controls (all $p < 0.05$) [13]. Interestingly, the left ventricular vortex area in severe ToF showed a mild but significant positive correlation with LV isovolumic relaxation time ($p = 0.038$) [13]. These findings strongly suggest that altered fetal intracardiac flow patterns may reflect early remodeling processes even before birth [13,14].

Similarly, in fetuses with coarctation of the aorta, Zhou et al. [15] studied 30 fetuses with CoA and 30 gestational-age-matched controls. Left ventricular vortex visualization was feasible in 93% of fetuses, confirming the applicability of BST in prenatal assessment. Fetuses with CoA showed significantly larger and wider left ventricular vortices than controls ($p < 0.05$) [15]. Vortex area was positively related to LV sphericity index ($r = 0.52$, $p = 0.003$) and isovolumic relaxation time ($r = 0.42$, $p = 0.021$), while a negative correlation was observed with mitral valve size ($r = -0.443$, $p = 0.014$) [15]. These data provide further evidence that BST can identify subtle fetal flow abnormalities associated with early ventricular remodeling [15].

Energy Loss

BST echocardiography has also been successfully applied to the assessment of right ventricular flow energetics [4]. In a cohort of 57 children in total, including 21 with repaired tetralogy of Fallot and severe pulmonary insufficiency, 11 with large atrial septal defects, and 25 healthy controls, right ventricular diastolic energy loss was similarly increased in both disease groups and significantly higher than in controls [4]. Interestingly, the spatial distribution of energy loss was highly informative: during systole, the highest values were localized at the right ventricular outflow tract, whereas during early diastole they were predominantly located around the tricuspid valve inflow region [4]. In patients with repaired tetralogy of Fallot, an additional apical early diastolic area of elevated energy loss was identified, corresponding to the collision between tricuspid inflow and pulmonary insufficiency jet, thus providing a clear pathophysiological correlate of flow inefficiency [4].

Intraventricular Pressure Difference

Another highly promising application of BST is the assessment of diastolic function through the estimation of intraventricular pressure difference (IVPD) [3,7,16]. In the study by Sørensen et al. [3], 138 controls, 10 patients with dilated cardiomyopathy, and 21 patients with hypertrophic cardiomyopathy younger than 18 years were analyzed. Mean IVPD during early diastole was significantly higher in controls (-2.28 ± 0.62 mmHg) compared with both dilated cardiomyopathy (-1.21 ± 0.39 mmHg, $p < 0.001$) and hypertrophic cardiomyopathy (-1.57 ± 0.47 mmHg, $p < 0.001$) [3]. Feasibility remained high across all groups, being 88.3% in controls, 80% in dilated cardiomyopathy, and 90.4% in hypertrophic cardiomyopathy, confirming the applicability of this technique even in structurally abnormal ventricles. These findings indicate a reduction in early diastolic suction in pediatric cardiomyopathies and support the use of BST-derived IVPD as a novel marker of diastolic dysfunction [3].

The physiological validity of this parameter has recently been further strengthened by the invasive validation study by Sørensen et al. [16], who compared BST-derived IVPD measurements with invasive micromanometer catheter measurements in an open-chest porcine model. Across 103 invasive measurements obtained in six pigs, BST-derived IVPD showed excellent agreement with invasive measurements, with a mean difference of -0.01 mmHg ($p = 0.33$) and a very high correlation coefficient ($r = 0.95$, $p < 0.001$) [16]. In the early clinical application, the authors analyzed 83 healthy controls and 44 pediatric patients with univentricular heart physiology. Feasibility was 93.9% in controls and 88.6% in UVH patients [16]. Median IVPD was significantly higher in controls than in UVH patients (-1.82 vs. -0.88 mmHg, $p < 0.001$), again supporting the concept of impaired diastolic suction in abnormal ventricular physiology [16].

3.3.2. BST for a Deeper Understanding of Complex CHD, Aortic and Pulmonary Flow Dynamics

BST may be employed as a complementary tool to color Doppler for a better and more intuitive understanding of flow dynamics across the cardiac chambers and main vessels [17,18]. Movie S2. BST may be helpful in understanding the turbulence occurring at the level of the main vessels due to stenosis, the formation of vortices after the stenosis, and their contribution to the post-stenotic dilatation [7,9,16,18]. Movie S3. Similarly, BST may be helpful for a deeper understanding of vortex formation and energy loss in heart chambers due to regurgitant flow [7,9,17,18]. Movies S4 and S5. Vortices in the stenotic vessels by vector flow imaging were first described by Honda and colleagues in 2014, in a 15-month-old baby with PS and post-stenotic dilatation [19]. The authors demonstrated that after percutaneous valvuloplasty, the MPA diameter, the vortex dimension, and the EL (energy loss) all diminish [19]. More recently, BST has been applied for the evaluation of stenotic and regurgitant semilunar valve disease, with a special focus on the aortic disease [17]. In Figure 2, we provide an example of vortex propagation in a child with pulmonary stenosis after pulmonary valvuloplasty. Figure 3.

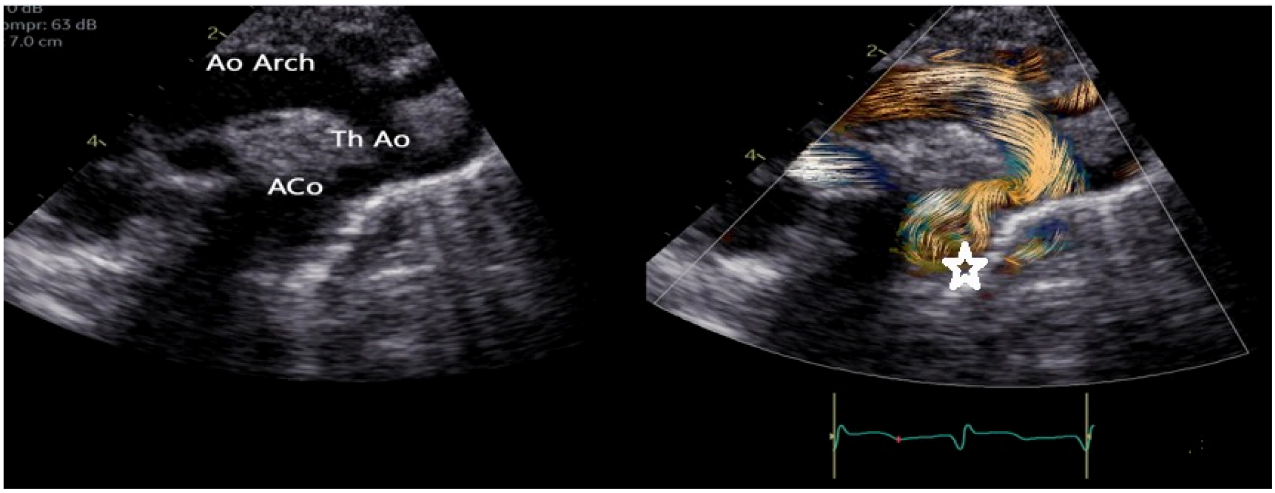


Figure 3. Parasternal view in a 2-day-old neonate with aortic coarctation. Vortex (star) forms at the level of post-stenotic dilatation.

3.3.3. Four-Dimensional Flow: A New Echocardiographic Semiotic: Vortex and Flow Signs as New Markers of Diseases

Vortices in Pathological Conditions

Under physiological conditions, vortices contribute to efficient blood transport and minimize energy loss. However, in the presence of structural cardiovascular abnormalities, vortex formation may reflect disturbed flow dynamics and altered hemodynamic conditions.

In cases of valvular or vascular stenosis, blood flow accelerates through the narrowed segment and becomes unstable distal to the obstruction. This results in the development of turbulent flow with a characteristic spiral motion, leading to the formation of a post-stenotic vortex. Such vortices are generated by flow separation and the dissipation of kinetic energy beyond the stenotic site and may vary in size and intensity according to the severity of the obstruction. Representative examples of post-stenotic vortex formation are shown in Figure 3 in a neonate with aortic coarctation. Vortices form at the level of post-stenotic dilatation.

Vortices may also arise in patients with congenital heart disease (CHD), particularly following surgical or interventional repair. Alterations in the geometry of cardiac chambers,

outflow tracts, or great vessels can create regions of abnormal flow acceleration and recirculation. For example, in patients with repaired perimembranous ventricular septal defects, a vortex can frequently be visualized within the left ventricular outflow tract adjacent to the ventricular septal patch. In this setting, local changes in ventricular geometry and flow direction generate turbulence and recirculating flow patterns that are readily identified by BST Figure 4.

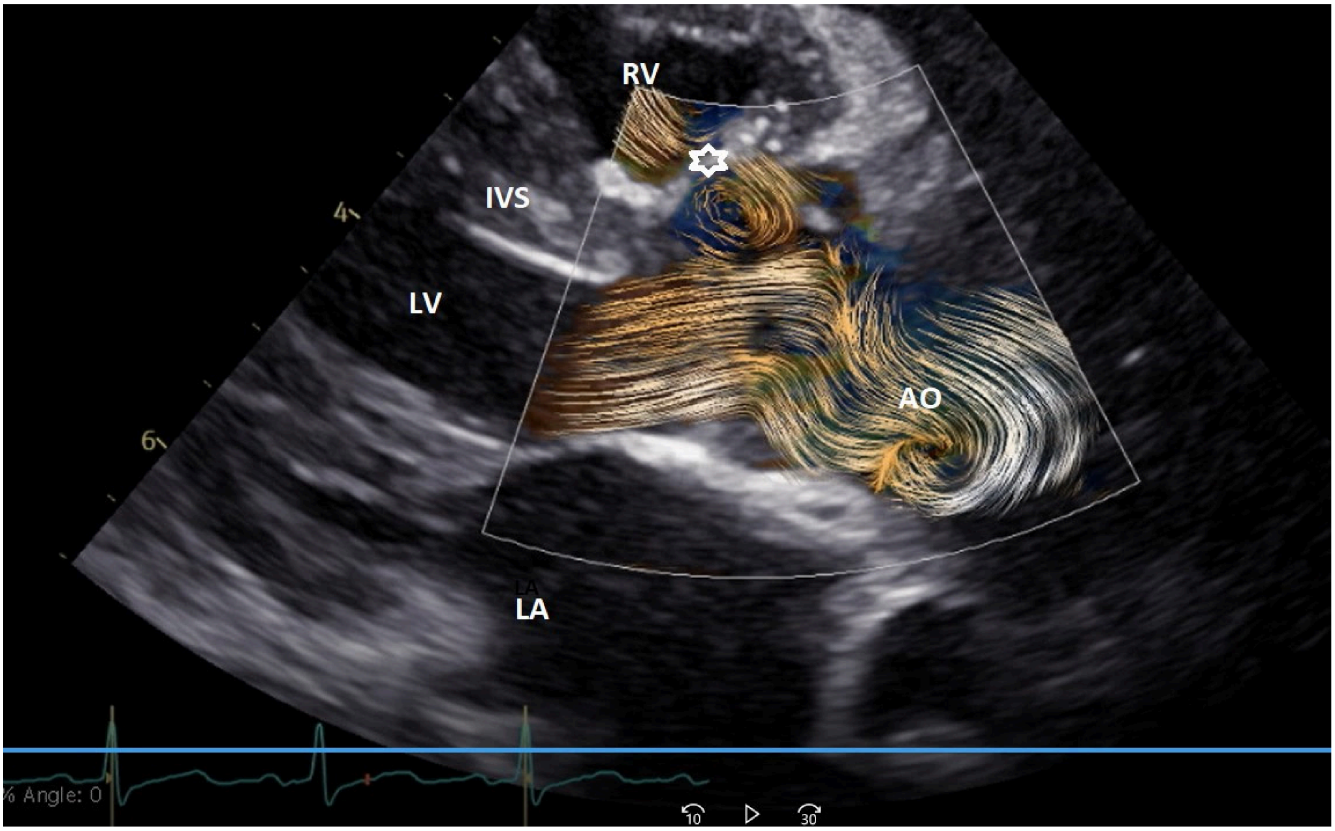


Figure 4. Parasternal view showing vortex formation in the left ventricular outflow tract of a 7-day-old child with repaired perimembranous VSD. The vortex can be visualized at the level of the patch (star). Ao = aorta, IVS = interventricular septum, LA = left atrium, LV = left ventricle, RV = right ventricle.

The Stop-Flow Sign

A provisional visual observation, referred to here as the "stop-flow sign," is the apparent abrupt interruption of a displayed blood-flow stream near a severe anatomical obstruction. In aortic coarctation, the forward-flow column may appear to terminate at the narrowing. This appearance has not been validated as a diagnostic sign or as a predictor of progression. Because an apparent interruption may also result from loss of speckle signal, tracking failure, imaging-plane limitations, or display/post-processing settings, it should not be interpreted as true cessation of flow without corroboration by conventional Doppler and other clinical imaging. In the illustrative cases, tracking continuity and signal quality should be reviewed frame by frame; the current material does not establish a validated method for excluding all such artifacts. Examples are shown in Figure 5.

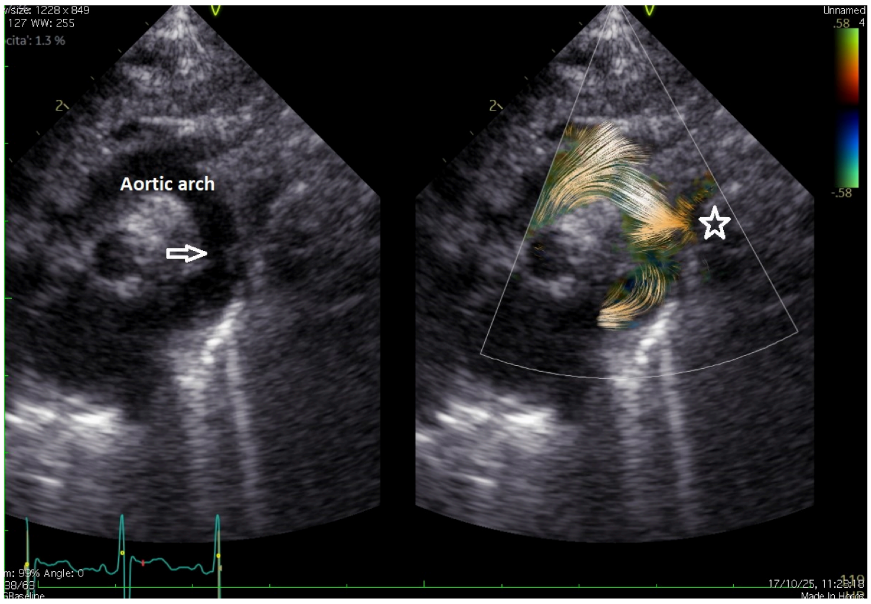


Figure 5. Suprasternal view of a 3-day-old neonate with mild aortic coarctation at the level of the isthmus (arrow). An apparent interruption of the displayed flow stream is shown (star). This illustrative observation is not a validated diagnostic or predictive sign; signal loss, tracking failure, and imaging-plane limitations cannot be excluded.

A similar appearance may be seen at the level of an atretic or severely hypoplastic pulmonary valve in pulmonary atresia, critical pulmonary stenosis, or tetralogy of Fallot with markedly reduced antegrade flow (Figure 6). At present, this should be described as an illustrative observation rather than a validated sign of absent flow or a marker of lesion severity. Confirmation with color and spectral Doppler, anatomical imaging, and clinical findings remains essential.

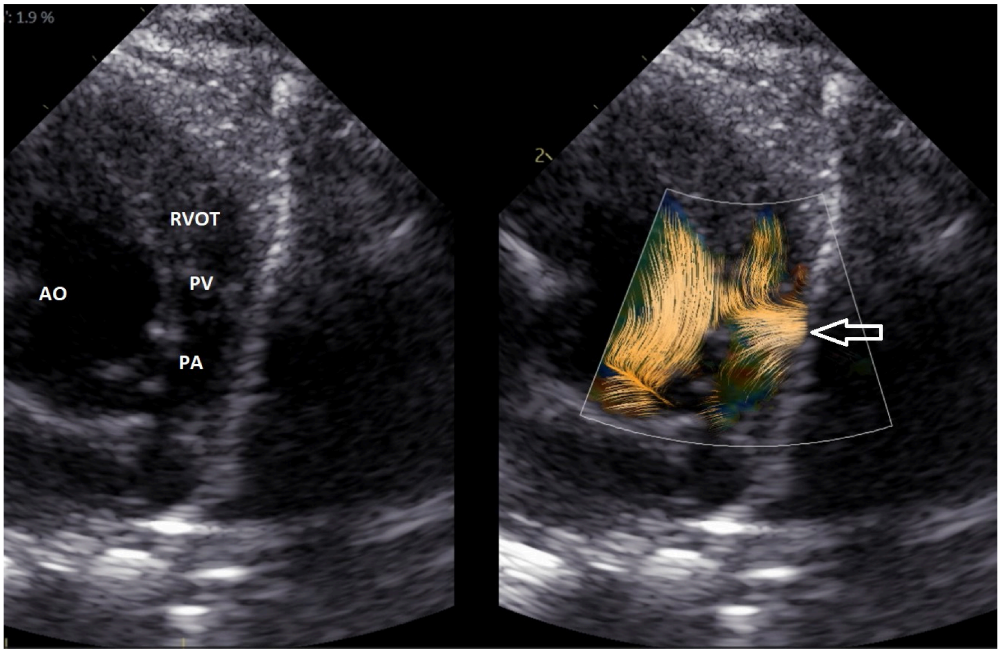


Figure 6. A 2-day-old neonate, 3 kg, with tetralogy of Fallot and a severely hypoplastic pulmonary valve. The anterograde flow is extremely limited, and the stop flow phenomenon can be observed. Ao = aorta, PA = pulmonary artery, PV = pulmonary valve, RVOT = right ventricle outflow tract.

3.3.4. Vortex in the Aorta

Physiologic flow in the aortic root and ascending aorta is laminar but not necessarily limited to the axial direction [9,17,20]. Indeed, helical and spiral flow within the aorta have been identified in both healthy and diseased aortas [9,17,20]. The formation of physiological vortices within the aortic sinuses of Valsalva is also well known [9,17,20,21], and was first hypothesized by Leonardo da Vinci [21]. In recent years, adult [20] and pediatric [22] cardiac MR studies have focused on the role of altered high-velocity, turbulent, helical flow hemodynamics in poststenotic dilatation in bicuspid aorta, which is now considered not only a genetic disorder but rather a sum of a genetic disorder and altered flow dynamics [20,22].

Application of BST echocardiography for the evaluation of aortic flow in children is still limited but promising [9,16]. In 100 healthy children [9], specific patterns of aortic flow by BST were observed. Initially, in early systole, the flow in the aortic root is laminar; however, in mid-systole, the flow splits into two helical branches going in opposite directions (one to the right ascending aortic wall and the other toward the left aortic wall), and vortices form close to the sino-tubular junction [9]. Finally, the flow returns laminar during late systole [9] (Figure 7). A study [17] of BST in over 14 children with bicuspid aortic valve (BAV) <10 years of age and 24 age-matched controls revealed how children with BAV exhibit altered flow dynamics in the aortic root and left ventricle in the absence of significant aortic root dilation [9]. Children with BAV [17] had on average higher aortic root vorticity (e.g., 25.9, 23.4–29.2 Hz vs. 17.8, 9.0–26.2 Hz, $p < 0.05$), vector complexity (e.g., 0.17, 0.14–0.31 vs. 0.05, 0.02–0.13, $p < 0.01$), and rate of energy loss (e.g., 7.9, 4.9–12.1 mW/m vs. 2.7, 1.2–7.4 mW/m, $p = 0.01$). In children with BAV furthermore there was higher LV average diastolic vorticity (e.g., 20.9 ± 5.8 Hz vs. 11.4 ± 5.2 Hz, $p < 0.01$), kinetic energy (e.g., 0.11 ± 0.05 J/m vs. 0.04 ± 0.02 J/m, $p < 0.01$), vector complexity (e.g., 0.38 ± 0.1 vs. 0.23 ± 0.1, $p < 0.01$), and rate of energy loss (e.g., 11.1 ± 4.8 mW/m vs. 2.7 ± 1.9 mW/m, $p < 0.01$ [17]. Practical examples of differences between physiological and pathological aortic vortices are provided in Figures 8–10 and Movies S6 and S7.

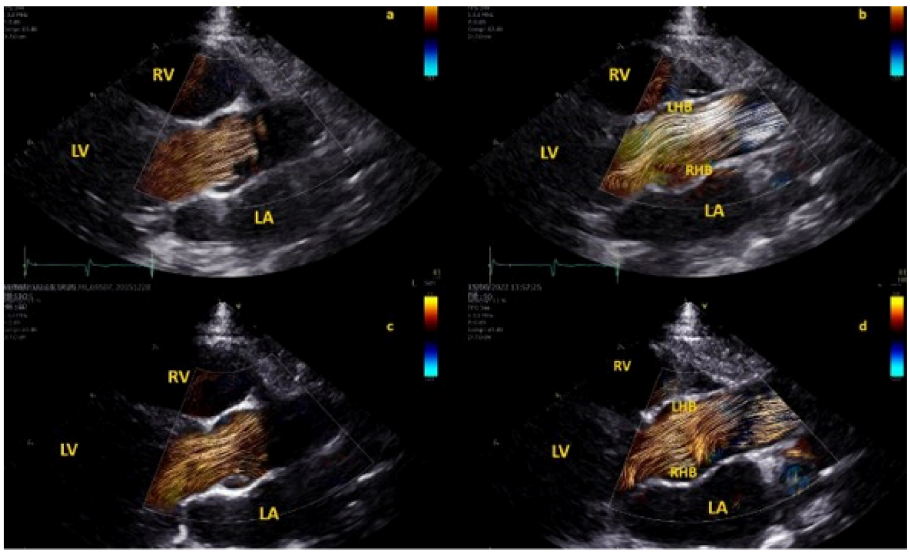


Figure 7. Phases of aortic flow during systole in normal subjects. Panel 1 illustrates early systole, during which blood flow within the aortic root remains laminar up to the level of the aortic cusp tips. Panel 2 demonstrates the division of flow into two counter-rotating helical streams: a right-handed helix directed toward the left aortic wall and a left-handed helix directed toward the right aortic wall. LA denotes left atrium; LHB, left-handed branch; LV, left ventricle; RHB, right-handed branch; and RV, right ventricle.

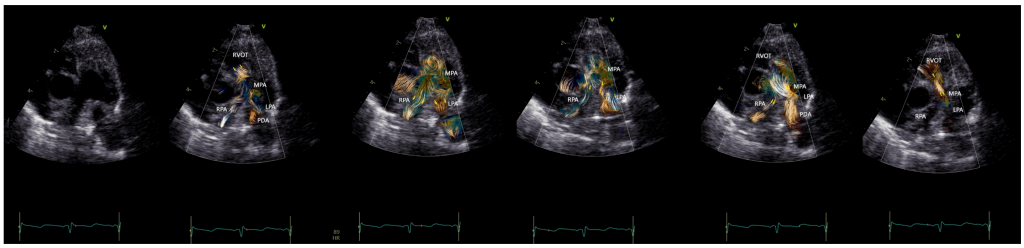


Figure 8. Propagation of vortical flow across the pulmonary valve in a neonate (weight 2.8 kg) with pulmonary stenosis. The short-axis view demonstrates vortex formation and its propagation into the pulmonary arteries throughout the cardiac cycle. Vortex formation at the level of the pulmonary valve at the onset of systole; propagation into the main pulmonary artery during mid-systole; further extension into the pulmonary artery branches during late systole and early diastole.



Figure 9. Movie S6: Vortical flow patterns in a patient with a bicuspid aortic valve causing moderate stenosis. The vortex develops at the end of diastole in both subjects. However, in the healthy subject (A), a physiologic vortex is confined within the aortic root (AoRoot). In contrast, in the child with a bicuspid aortic valve (B), the presence of stenosis leads to a more distally located vortex, developing above the sinutubular junction, with greater size compared to the normal counterpart.

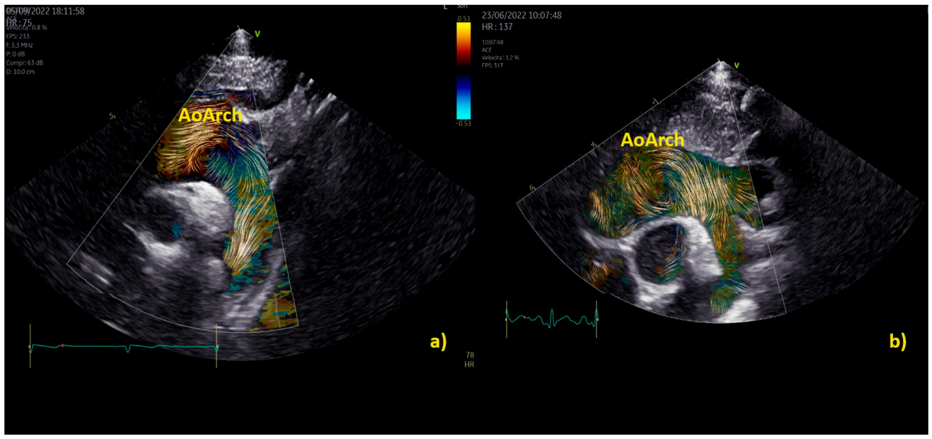


Figure 10. Vortex formation in the aortic arch of a healthy child (**a**) and in a 2-year-old child with moderate aortic valve stenosis (**b**). In the healthy subject (**a**), the vortex is smaller in extent and is confined to the ventral aspect of the aortic arch, below the origin of the first two epi-aortic branches. In contrast, in the child with valvular stenosis (**b**), the vortex is larger and more extensive, originating proximal to the epi-aortic branches and occupying a substantial portion of a dilated transverse aortic arch.

This concept is further reinforced by fetal studies. Zhou et al. [14] evaluated 35 fetuses with ToF and 35 controls and found vortex flow in the ascending aorta in 91.4% of ToF fetuses compared with only 17.1% of controls ($p < 0.001$). The median number of vortices was also significantly higher in ToF ($p < 0.001$) [14]. Interestingly, the presence of vortices correlated significantly with aortic valve size ($r = 0.54$, $p = 0.001$) and inversely with the LV inflow–outflow angle ($r = -0.376$, $p = 0.026$), suggesting an important interaction between geometry and flow organization already in fetal life [14].

3.3.5. Univentricular Heart

Recent evidence on intracavitary flow assessment in univentricular physiology indicates that blood speckle tracking (BST), vector flow mapping, and computational fluid dynamics (CFD) consistently identify less efficient vortex formation in systemic right ventricles compared with single left ventricles [23–26]. Available studies remain exploratory and are characterized by small sample sizes. For example, Grünwald et al. [23] analyzed a cohort of 7 children (5 with single right ventricle and 2 healthy controls, age 4–15 years) using a multimodality workflow integrating 3D echocardiography-derived geometries, mesh conversion through Image Arena and MATLAB R2025a into STL format, smoothing with Blender, and moving-mesh CFD simulations in ANSYS Fluent 2025 R1 with a k–ω SST turbulence model to quantify vortex formation time (VFT), turbulent kinetic energy (TKE), and ventricular washout efficiency [23]. Their results demonstrated significantly reduced VFT and TKE in single right ventricle patients, together with impaired apical vortex propagation and lower washout efficiency, supporting the presence of deteriorated diastolic flow organization [23]. Similarly, in a prospective observational study by Akiyama K et al. [27], 10 patients were enrolled (5 single right ventricle and 5 single left ventricle), and intraoperative transesophageal 2D color Doppler cine loops were analyzed with vector flow mapping software (Hitachi Aloka Medical, Tokyo, Japan) to quantify intraventricular energy loss, kinetic energy of outflow, and mean diastolic vorticity. Although energy loss did not differ significantly between groups (24.8 [22.1–30.2] vs. 37.6 [27.2–38.6] mW/m, $p = 0.09$), kinetic energy was significantly lower in the single right ventricle group (16.3 [9.2–17.5] vs. 75.8 [74.9–142.5] mW/m, $p < 0.05$), as was diastolic vorticity (228.4 [196.9–282.5] vs. 332.2 [330.6–530.8] s^{-1}, $p < 0.05$), confirming a less coherent and energetically less efficient vortex pattern [27]. Overall [23–25], despite methodological heterogeneity and limited statistical power, these studies consistently support impaired vortex dynamics in systemic right ventricle physiology, suggesting that BST-derived and CFD-based flow metrics may serve as emerging imaging biomarkers for hemodynamic inefficiency and longitudinal risk stratification in congenital single ventricle disease [23–26]. The use of BST furthermore may be extended for a deeper understanding of complex flow dynamics of valve regurgitation and Glenn and TCPC conduit circuits (Movie S8).

3.4. Summary of Current Evidence

Current evidence supports blood speckle tracking echocardiography as a highly promising complementary imaging modality for the advanced assessment of cardiovascular flow dynamics in pediatric and fetal congenital heart disease [1–9]. Across the available literature, BST has consistently demonstrated high feasibility [1,8], with acquisition success rates generally above 90% in both healthy children and patients with CHD, supporting its integration into routine pediatric echocardiographic workflows, particularly in superficial structures and small body sizes [1,8].

The strongest evidence currently relates to the characterization of ventricular vortex morphology and flow energetics [1–9]. Multiple studies have shown that altered ventricular geometry and abnormal loading conditions are associated with significant modifications

in vortex size, position, persistence, and energetic efficiency [5,8,13,19]. In both fetal and postnatal CHD populations, enlarged or displaced vortices have been associated with ventricular remodeling, impaired diastolic performance, and abnormal chamber sphericity indices [5,13,14]. Similarly, BST-derived energy loss and kinetic energy measurements have provided novel mechanistic insights into flow inefficiency in conditions such as repaired tetralogy of Fallot [5,13], pulmonary regurgitation [5,13], and bicuspid aortic valve disease [17].

Another area of robust evidence concerns diastolic functional assessment through BST-derived intraventricular pressure differences (IVPD) [3,15]. Both clinical and invasive validation studies have demonstrated excellent agreement between BST-derived and catheter-based measurements, supporting the physiological reliability of this technique as a novel marker of ventricular suction and diastolic dysfunction [3,16]. Reduced IVPD values have been consistently reported in pediatric cardiomyopathies and univentricular physiology [3,16].

Emerging evidence also suggests an important role for BST in the study of great vessel hemodynamics, particularly in the aortic root, ascending aorta, and pulmonary arteries, where abnormal helical flow, post-stenotic vortices, and increased energy loss may contribute to vascular remodeling and post-stenotic dilatation [9,20,21]. This is particularly relevant in bicuspid aortic valve disease and semilunar valve stenosis [9,18,19].

In complex congenital heart disease, including single-ventricle physiology, small exploratory studies [23,26,27] using different flow-imaging methods have described altered vortex formation and flow efficiency. These findings are hypothesis-generating and do not establish that BST-derived metrics distinguish systemic right from systemic left ventricles or predict longitudinal outcomes.

Overall, although current evidence remains largely based on single-center observational studies with relatively small sample sizes [1–9,12–18,23,24,27], BST has provided useful pathophysiological illustrations and may complement conventional Doppler imaging; however, incremental diagnostic value and any prognostic benefit have not yet been established in adequately powered comparative studies [1–9]. Larger multicenter prospective studies are now required to establish normative data, reproducibility standards, and its potential diagnostic and prognostic impact.

3.5. Future Directions

Once quantification tools become widely available, BST may represent a breakthrough in the assessment and understanding of pathophysiological mechanisms in CHD. In particular, the quantification of energy loss and interventricular pressure differences may open new avenues for the early diagnosis and management of children with congenital heart disease, including those with a univentricular heart [1–9], as well as cardiomyopathies [3]. The commercial availability of software already developed for research purposes [3,4,16] is highly anticipated and strongly encouraged by the scientific community, together with the development of large-scale studies aimed at validating the diagnostic and prognostic significance of the novel parameters derived from BST in comparison with conventional echocardiographic techniques.

3.6. Other 4D Flow Echocardiographic Techniques

The Hyper Doppler

Hyper Doppler is a novel echocardiographic technique that allows noninvasive assessment of intracardiac flow dynamics using conventional color Doppler imaging combined with advanced fluid-dynamic reconstruction algorithms (28–29). The technique is based on the reconstruction of two-dimensional intracavitary velocity fields from standard color

Doppler datasets through the application of fluid mechanics principles (28–29). Dedicated software generates vector flow maps that enable visualization and quantification of vortex dynamics during the cardiac cycle (28–29). Several parameters can be derived, including vortex area, circulation, kinetic energy dissipation, vorticity, and hemodynamic forces, providing insight into ventricular efficiency and blood flow organization (28–29).

In the first clinical application, Fiorencis et al. [28] reported a feasibility cohort of 200 consecutive patients and additional groups comprising 50 healthy subjects, 30 athletes, and 50 patients with heart failure. Importantly, normalized kinetic energy dissipation was lower in patients with heart failure than in healthy subjects; the direction of this finding should not be reversed. Subsequently, Sabatino et al. [29] studied 120 patients with severe aortic stenosis, 60 with concentric ventricular remodeling, and 100 controls. The study description should reflect these groups rather than a cohort of 113 patients or a comparison between severe and moderate stenosis. These findings provide preliminary evidence that Hyper Doppler can characterize differences in intracardiac flow, but their diagnostic and prognostic implications remain to be established.

Although both Hyper Doppler (28–29) and Blood Speckle Tracking (BST) (1–4) aim to characterize intracardiac flow dynamics using echocardiography, they are based on different physical principles and provide partially complementary information. BST directly tracks the motion of blood speckles (natural acoustic markers generated by red blood cell aggregates) within high-frame-rate ultrasound images, allowing a relatively direct visualization of blood flow patterns and vortex formation (1–4). In contrast, Hyper Doppler (28–29) reconstructs intraventricular flow fields from conventional color Doppler data using fluid-dynamic algorithms and mathematical modeling, deriving vector flow maps and quantitative indices such as vorticity, circulation, kinetic energy dissipation, and hemodynamic forces. Consequently, BST (1–4) is more dependent on high-quality blood speckle visualization and dedicated high-frame-rate imaging, whereas Hyper Doppler (28–29) can be applied retrospectively to standard color Doppler acquisitions and is more easily integrated into routine clinical examinations. However, both techniques currently rely predominantly on two-dimensional flow analysis. They therefore sample only the imaged plane and cannot fully capture out-of-plane velocity components or reconstruct the complete three-dimensional flow field. Apparent vortices and flow discontinuities may consequently depend on the selected imaging plane, temporal resolution, signal quality, tracking settings, and post-processing. Further studies are needed to clarify their relative diagnostic and prognostic value and to establish their role in clinical practice.

4. Conclusions

Blood speckle tracking is a newer and potentially revolutionary echocardiographic imaging technique allowing a unique visualization of blood flow trajectories and vortex formation in cardiac chambers and main vessels, which may open to a wider and more comprehensive understanding of complex flow dynamics, such as those in CHDs. BST applications and use, however, remain underestimated due to the limited quantification tools currently available and limited clinical evidence on the advantages of its use. Software for BST quantification, already developed for research purposes, is eagerly anticipated for commercial release to fully harness the potential of this novel and potentially revolutionary technique.

Supplementary Materials: The following supporting information can be downloaded at: https://www.mdpi.com/article/10.3390/jcm15228966/s1, All blood speckle tracking (BST) movies and figures were acquired in non-sedated infants at frame rates of 400–500 fps. Clips encompassing two cardiac cycles were stored using medium (66 cm/s) to low (53 cm/s) Nyquist limits. Supplementary Movie S1 shows the normal diastolic vortex within the left ventricle (LV) in a healthy heart. Supple-

mentary Movie S2: A transposition of the great arteries with restrictive patent foramen ovale (PFO). Supplementary Movie S3: Turbulent flow across the pulmonary valve of a neonate with pulmonary stenosis. The turbulence is propagated to the pulmonary arteries. Supplementary Movie S4: free pulmonary regurgitation in a neonate with tetralogy of Fallot with absent pulmonary valve. Supplementary Movie S5: Severe tricuspid regurgitation in hypoplastic left heart syndrome (HLHS) after Norwood operation is visualized by BST. Supplementary Movie S6: Vortical flow patterns in a patient with a bicuspid aortic valve causing moderate stenosis. The vortex develops at the end of diastole in both subjects. However, in the healthy subject (A), a physiologic vortex is confined within the aortic root (AoRoot). In contrast, in the child with a bicuspid aortic valve (B), the presence of stenosis leads to a more distally located vortex, developing above the sinutubular junction, with greater size compared to the normal counterpart. Abbreviations: AoRoot = aortic root; LA = left atrium; LV = left ventricle; MV = mitral valve; RA = right atrium; RV = right ventricle. Supplementary Movie S7: Vortex formation in the aortic arch of a healthy child (A) and in a 2-year-old child with moderate aortic valve stenosis (B). In the healthy subject (A), the vortex is smaller in extent and is confined to the ventral aspect of the aortic arch, below the origin of the first two epi-aortic branches. In contrast, in the child with valvular stenosis (B), the vortex is larger and more extensive, originating proximal to the epi-aortic branches and occupying a substantial portion of a dilated transverse aortic arch. Supplementary Movie S8: the flow across the Glenn circuit is well shown by BST. The flow direction is nicely visualized by arrows (Figure 7). Current Figures 2 and 10 reproduce images appearing in Figures 2 and 6 of the previous publication (10). (doi:10.3390/healthcare12020263).

Author Contributions: M.C. idealization and writing, P.M. and G.C. (Guglielmo Capponi) data collecting; E.F., C.V. and G.C. (Giulia Corana) data collecting and analysis, G.S. and N.A. supervision. All authors have read and agreed to the published version of the manuscript..

Funding: This research received no external funding.

Data Availability Statement: No new data were created or analyzed in this study.

Conflicts of Interest: The authors declare no conflicts of interest.

References

1. Nyrnes, S.A.; Fadnes, S.; Wigen, M.S.; Mertens, L.; Lovstakken, L. Blood Speckle-Tracking Based on High-Frame Rate Ultrasound Imaging in Pediatric Cardiology. *J. Am. Soc. Echocardiogr.* **2020**, *33*, 493–503.e5. [CrossRef] [PubMed]
2. Cantinotti, M.; Marchese, P.; Koestenberger, M.; Giordano, R.; Santoro, G.; Assanta, N.; Kutty, S. Intracardiac flow visualization using high-frame rate blood speckle tracking echocardiography: Illustrations from infants with congenital heart disease. *Echocardiography* **2021**, *38*, 707–715. [CrossRef] [PubMed]
3. Sørensen, K.; Fadnes, S.; Mertens, L.; Henry, M.; Segers, P.; Løvstakken, L.; Nyrnes, S.A. Assessment of Early Diastolic Intraventricular Pressure Difference in Children by Blood Speckle-Tracking Echocardiography. *J. Am. Soc. Echocardiogr.* **2023**, *36*, 523–532.e3. [CrossRef] [PubMed]
4. Mawad, W.; Løvstakken, L.; Fadnes, S.; Grønli, T.; Segers, P.; Mertens, L.; Nyrnes, S.A. Right Ventricular Flow Dynamics in Dilated Right Ventricles: Energy Loss Estimation Based on Blood Speckle Tracking Echocardiography—A Pilot Study in Children. *Ultrasound Med. Biol.* **2021**, *47*, 1514–1527. [CrossRef] [PubMed]
5. Meyers, B.; Nyce, J.; Zhang, J.; Frank, L.H.; Balaras, E.; Vlachos, P.P.; Loke, Y.H. Intracardiac Flow Analysis of the Right Ventricle in Pediatric Patients with Repaired Tetralogy of Fallot Using a Novel Color Doppler Velocity Reconstruction. *J. Am. Soc. Echocardiogr.* **2023**, *36*, 644–653. [CrossRef] [PubMed]
6. de Waal, K.; Crendal, E.; Boyle, A. Left ventricular vortex formation in preterm infants assessed by blood speckle imaging. *Echocardiography* **2019**, *36*, 1364–1371. [CrossRef] [PubMed]
7. Borrelli, N.; Avesani, M.; Sabatino, J.; Ibrahim, A.; Josen, M.; Paredes, J.; Di Salvo, G. Blood speckle imaging: A new echocardiographic approach to study fluid dynamics in congenital heart disease. *Int. J. Cardiol.* **2021**, *2*, 100079. [CrossRef]
8. Marchese, P.; Cantinotti, M.; Van den Eynde, J.; Assanta, N.; Franchi, E.; Pak, V.; Santoro, G.; Koestenberger, M.; Kutty, S. Left ventricular vortex analysis by high-frame rate blood speckle tracking echocardiography in healthy children and in congenital heart disease. *Int. J. Cardiol. Heart Vasc.* **2021**, *37*, 100897. [CrossRef] [PubMed]
9. Cantinotti, M.; Marchese, P.; Scalese, M.; Giordano, R.; Franchi, E.; Assanta, N.; Koestenberger, M.; Barnes, B.T.; Celi, S.; Jani, V.; et al. Characterization of Aortic Flow Patterns by High-Frame-Rate Blood Speckle Tracking Echocardiography in Children. *J. Am. Heart Assoc.* **2023**, *12*, e026335. [CrossRef] [PubMed]

10. Cantinotti, M.; Marchese, P.; Franchi, E.; Santoro, G.; Assanta, N.; Giordano, R. Four-Dimensional Flow Echocardiography: Blood Speckle Tracking in Congenital Heart Disease: How to Apply, How to Interpret, What Is Feasible, and What Is Missing Still. *Healthcare* **2024**, *12*, 263. [CrossRef] [PubMed]
11. Available online: https://www.prisma-statement.org/prisma-2020 (accessed on 1 January 2026).
12. Villeman, O.; Baranger, J.; Friedberg, M.K.; Papadacci, C.; Dizeux, A.; Messas, E.; Tanter, M.; Pernot, M.; Mertens, L. Ultrafast Ultrasound Imaging in Pediatric and Adult Cardiology: Techniques, Applications, and Perspectives. *JACC Cardiovasc. Imag.* **2020**, *13*, 1771–1791.
13. Liu, Y.; Zhou, D.; Yang, Y.; Yang, P.; Song, S.; Zeng, S. Vortex formation of cardiac bilateral ventricles in fetuses with tetralogy of Fallot assessed by blood speckle-tracking echocardiography. *BMC Pregnancy Childbirth* **2025**, *25*, 1279. [CrossRef] [PubMed]
14. Zhou, D.; Liu, Y.; Xu, G.; Yang, Y.; Zeng, S. Abnormal flow patterns in ascending aorta in fetuses with tetralogy of Fallot: Evaluation by blood speckle-tracking echocardiography. *Ultrasound Obstet. Gynecol.* **2025**, *66*, 614–620. [CrossRef] [PubMed]
15. Zhou, D.; Xu, R.; Liu, Y.; Yang, Y.; Wu, Z.; Luo, Y.; Zeng, S. Left Ventricular Vortex Characteristics in Fetuses with Coarctation of the Aorta by Blood Speckle-Tracking Echocardiography. *J. Ultrasound Med.* **2024**, *43*, 841–849. [CrossRef] [PubMed]
16. Sørensen, K.; Fadnes, S.; Mawad, W.; Henry, M.; Flade, H.M.; Østvik, A.; Myklebust, T.Å.; Kirkeby-Garstad, I.; Løvstakken, L.; Mertens, L.; et al. Intraventricular pressure difference estimation based on blood speckle tracking-invasive validation and early clinical application. *Eur. Heart J. Cardiovasc. Imaging* **2025**, *26*, 1346–1357. [CrossRef] [PubMed]
17. Henry, M.; Fadnes, S.; Løvstakken, L.L.; Mawad, W.; Mertens, L.; Nyrnes, S.A. Flow Dynamics in Children with Bicuspid Aortic Valve: A Blood Speckle Tracking Study. *Ultrasound Med. Biol.* **2023**, *10*, 2354–2360. [CrossRef] [PubMed]
18. Fadnes, S.; Nyrnes, S.A.; Torp, H.; Lovstakken, L. Shunt flow evaluation in congenital heart disease based on two-dimensional speckle tracking. *Ultrasound Med. Biol.* **2014**, *40*, 2379–2391. [CrossRef] [PubMed]
19. Honda, T.; Itatani, K.; Miyaji, K.; Ishii, M. Assessment of the vortex flow in the post-stenotic dilatation above the pulmonary valve stenosis in an infant using echocardiography vector flow mapping. *Eur. Heart J.* **2014**, *35*, 306. [CrossRef] [PubMed]
20. Rodríguez-Palomares, J.F.; Dux-Santoy, L.; Guala, A.; Kale, R.; Maldonado, G.; Teixidó-Turà, G.; Galian, L.; Huguet, M.; Valente, F.; Gutiérrez, L.; et al. Aortic flow patterns and wall shear stress maps by 4D-flow cardiovascular magnetic resonance in the assessment of aortic dilatation in bicuspid aortic valve disease. *J. Cardiovasc. Magn. Reson.* **2021**, *20*, 28.
21. Ghraib, M.; Kremers, D.; Koochesfahani, M.; Kemp, M. Leonardo's vision of flow visualization. *Exp. Fluids* **2002**, *33*, 219–223. [CrossRef]
22. Rose, M.J.; Rigsby, C.K.; Berhane, H.; Bollache, E.; Jarvis, K.; Barker, A.J.; Schnell, S.; Allen, B.D.; Robinson, J.D.; Markl, M. 4-D flow MRI aortic 3-D hemodynamics and wall shear stress remain stable over short-term follow-up in pediatric and young adult patients with bicuspid aortic valve. *Pediatr. Radiol.* **2019**, *49*, 57–67. [CrossRef] [PubMed]
23. Grünwald, A.; Korte, J.; Wilmanns, N.; Winkler, C.; Linden, K.; Herberg, U.; Groß-Hardt, S.; Steinseifer, U.; Neidlin, M. Intraventricular Flow Simulations in Singular Right Ventricles Reveal Deteriorated Washout and Low Vortex Formation. *Cardiovasc. Eng. Technol.* **2022**, *13*, 495–503. [CrossRef] [PubMed]
24. Kheradvar, A.; Rickers, C.; Morisawa, D.; Kim, M.; Hong, G.R.; Pedrizzetti, G. Diagnostic and prognostic significance of cardiovascular vortex formation. *J. Cardiol.* **2019**, *74*, 403–411. [CrossRef] [PubMed]
25. Hong, G.R.; Pedrizzetti, G.; Tonti, G.; Li, P.; Wei, Z.; Kim, J.K.; Baweja, A.; Liu, S.; Chung, N.; Houle, H.; et al. Characterization and quantification of vortex flow in the human left ventricle by contrast echocardiography using vector particle image velocimetry. *JACC Cardiovasc. Imaging* **2008**, *1*, 705–717. [CrossRef] [PubMed]
26. Lampropoulos, K.; Budts, W.; Van de Bruaene, A.; Troost, E.; van Melle, J.P. Visualization of the intracavitary blood flow in systemic ventricles of Fontan patients by contrast echocardiography using particle image velocimetry. *Cardiovasc. Ultrasound* **2012**, *10*, 5. [CrossRef] [PubMed]
27. Akiyama, K.; Itatani, K.; Wu, I.Y.; Tachibana, Y.; Obata, Y.; Nakajima, Y.; Yamagishi, M.; Takayama, H.; Sawa, T. Difference in Intraventricular Vortex Between the Single Right Ventricle and Single Left Ventricle. *J. Cardiothorac. Vasc. Anesth.* **2021**, *35*, 2242–2243. [CrossRef] [PubMed]
28. Fiorencis, A.; Pepe, M.; Smarrazzo, V.; Martini, M.; Severino, S.; Pergola, V.; Evangelista, M.; Incarnato, P.; Previtero, M.; Maglione, M.; et al. Noninvasive Evaluation of Intraventricular Flow Dynamics by the HyperDoppler Technique: First Application to Normal Subjects, Athletes, and Patients with Heart Failure. *J. Clin. Med.* **2022**, *11*, 2216. [CrossRef] [PubMed]
29. Sabatino, J.; Leo, I.; Strangio, A.; La Bella, S.; De Sarro, R.; Montemurro, V.; Pedrizzetti, G.; Troilo, F.; Maglione, M.; Torella, D.; et al. Changes of intracardiac flow dynamics measured by HyperDoppler in patients with aortic stenosis. *Eur. Heart J. Open* **2024**, *4*, oeae069. [CrossRef] [PubMed]

Disclaimer/Publisher's Note: The statements, opinions and data contained in all publications are solely those of the individual author(s) and contributor(s) and not of MDPI and/or the editor(s). MDPI and/or the editor(s) disclaim responsibility for any injury to people or property resulting from any ideas, methods, instructions or products referred to in the content.